PHYSICAL REVIEW B VOLUME 41, NUMBER 5 15 FEBRUARY 1990-I

Self-consistent dipole theory of heterojunction band offsets

W. R. L. Lambrecht and B. Segall
Department of Physics, Case Western Reserve University, Cleveland, Ohio 44106

O. K. Andersen
Max-Planck-Institut für Festkörperforschung, Postfach 80 06 65, D-7000 Stuttgart 80, Federal Republic of Germany

(Received 22 May 1989)

A theory of heterojunction band offsets is developed within the density-functional framework in the local-density approximation. The linear-muffin-tin-orbital method is used in conjunction with a superlattice geometry for solving Schrödinger's equation of the heterojunction. The potential is constructed within the atomic-sphere approximation. Within this context the long-range electrostatics reduce to that of point charges, and the average electrostatic potential of the latter can be used as a local reference level. It is shown that, starting from an arbitrary alignment of the bulk potentials, the correct potential alignment is obtained by minimizing the total energy with respect to a *single* parameter: the interface dipole. This minimization is equivalent to screening the initially induced dipole by the macroscopic dielectric constant of the interface region of the heterojunction, which can be identified approximately with the harmonic average of the dielectric constants of the two semiconductors. The conditions under which this is valid are discussed. The calculations are performed within a so-called *frozen-shape* approximation, allowing the potentials to vary only by constant shifts. Almost perfect agreement between calculations using a *different* shift per atomic layer and calculations using a *single* shift per semiconductor provide a numerical demonstration that the self-consistent dipole is independent of the details of the dipole profile. They also show that the macroscopic dielectric constant of the heterojunction in the vicinity of the interface can be obtained with reasonable accuracy from the single-parameter variational calculation itself. The calculations also show that linear response is valid over a wide range. The theory is applied to an extensive set of lattice-matched semiconductor (110) interfaces and shown to be in excellent agreement with experimental results and previous more-involved calculations where available. The consequences of the present theory for interface-orientation dependence and metal-semiconductor interfaces are briefly discussed.

I. INTRODUCTION

When two solids are joined in a heterojunction or bicrystal, the electronic structure is perturbed locally near the interface, but a few layers away from the interface it reduces to that of the individual solids. One of the fundamental problems for such a system is how the two band structures line up in energy with respect to each other. For metal-metal contacts this problem is trivial because it follows from the alignment of the Fermi levels. When at least one of the solids is a semiconductor or insulator, however, this is not so, because the alignment of the chemical potentials only applies to the truly asymptotic situation. Closer to the interface, a region may exist where the local electronic structure is bulklike but with a different alignment. In fact, as will be shown, this occurs within a few atomic layers. It is this intermediate range alignment we will be concerned with in this paper and which is conventionally called the band discontinuity or band offset. In semiconductors or insulators, the macroscopic alignment of the chemical potential is accomplished by ionizing impurity levels and thus establishing depletion layers and associated band bending. As this phenomenon occurs over a length scale of several 100–1000 Å, depending on the doping concentrations, in contrast to the band discontinuity, which is established within a few atomic layers, it is essentially independent of the latter and will not be further considered in this paper.

The band discontinuities are of great technological importance both for metal-semiconductor and semiconductor-semiconductor contacts. The Schottky barrier in the former case and the conduction-band and valence-band offsets in the latter are key parameters in determining the electrical and optical properties of heterostructures and superlattices, which form the basis of many new electronic devices. In the following we will focus on semiconductor heterojunctions, though several aspects of the theory apply to metal-semiconductor contacts as well. Because of its importance, this topic has been the subject of numerous theoretical[1–21] and experimental[22–40] studies in recent years. Still, considerable confusion and controversies about the problem persist. The general framework adopted in the present theory of band offsets is the density-functional method. A general analysis of some of the most controversial aspects of the theory as well as calculations for a wide range of systems

 ©1990 The American Physical Society

is presented.

One of the most confusing points about band offsets is the question of whether a meaningful absolute reference level exists. Very much related is the question of how to decompose the band offset into an intrinsic bulk contribution and an interface dipole correction. Several authors have emphasized the role of electronic screening of the interface dipoles,[6-13] but it has not always been stated explicitly "what is to be screened" and "which dielectric constant" is applicable. In our opinion, much of the confusion is semantic in origin and due to unclear definitions of the terms *charge transfer, dipole,* etc. Another, but also related, controversial point is whether band offsets depend on the interface orientation. Finally, the use of the local-density-functional Kohn-Sham eigenvalues for band offsets has been questioned.[41,42]

Although it has already been pointed out by several authors, we here stress again that any separation of the band offset into a bulk contribution and a dipole correction is in principle arbitrary and hence has no special physical meaning. This is due to the nonuniqueness of the average electrostatic potential in an infinite periodic solid.[43] Choosing a reference level for the individual solids is thus a question of convenience related to the computational procedure employed. The choice made in the present paper is the average electrostatic potential of the point charges related to the atomic-sphere approximation (ASA), well known in the linear-muffin-tin-orbital (LMTO) method,[44] which is used for the present calculations. Once this point-charge potential is fixed on an absolute scale by choosing its average to be zero, the ASA potential is completely determined. We will refer to this choice as the ASA reference level. The dipole potential (henceforth called simply the *dipole*) of the heterojunction in this context is defined as the difference between the two asymptotic values of the average *point-charge* potential at both sides of the heterojunction:

$$D=\lim_{z\to\infty}V(z)-\lim_{z\to-\infty}V(z)\ . \tag{1}$$

Throughout this paper, we use Hartree atomic units ($e=\hbar=m=1$). V will be used to indicate the point-charge potential and v for the full potential. For clarity, we emphasize that the reference level is not needed in an absolute sense but only as a local characteristic of the periodic potential in the two asymptotic regions where the potential becomes bulklike. The bulk potentials aligned with respect to this reference level may be related to an interface-dependent reference charge density based on the bulk charge densities (see Sec. II B). This is a useful concept for discussing the origin of band offsets, but not essential in the computational procedure.

The most important result proved in this paper is that the dipole is the *only* relevant degree of freedom for the band offset. This means that instead of performing a fully self-consistent calculation, one need only carry out a single-parameter variational calculation to determine the band offset. The argument used to prove this result is based on linear-response theory, although it can be generalized beyond linear response. It shows that the initially induced dipole is screened by the *macroscopic* dielectric constant of the heterojunction, i.e., the dielectric constant of a sufficiently wide region in the vicinity of the interface (larger than the screening length so that outside this region the charge density is unperturbed). By initially induced dipole we mean the output dipole of the first iteration, i.e., the dipole resulting from Poisson's equation calculated from the charge density obtained from solving Schrödinger's equation with the reference potential as input. This assumes that the initial alignment is within the linear-response range of the correct alignment. Eventually one may get within the linear-response range by successive iterations. Utilizing this requires either that the dielectric constant of the heterojunction is known, or that the variational calculation describes the dielectric screening correctly. As will be shown by the numerical calculations, linear response is valid over a wide range and thus the first condition is easily satisfied. In particular, it is very well satisfied using the ASA reference level. Second, our calculated dielectric constants are shown to be in very good agreement with appropriate averages of the experimental values of the dielectric constants of the semiconductors involved in the heterojunction. The discrepancies can be largely ascribed to the use of the local-density approximation (LDA) for exchange and correlation. This shows that the single-parameter calculation not only is a valid procedure when the dielectric response is known, but is in fact also sufficient, in practice, to calculate the macroscopic dielectric response. It is pointed out that the dielectric response is essentially the curvature or second derivative of the total energy. The approximate independence of short-range versus long-range screening allows one to obtain the correct long-range behavior even without self-consistency of the short-range behavior.

In practice, we use a so-called *frozen-shape* approximation, in which the potential wells within the Wigner-Seitz spheres, characteristic of the ASA-LMTO method, have the same radial dependence as in the respective self-consistently calculated bulk solids. They are allowed to vary only by a constant shift. The single-parameter calculation mentioned above corresponds to the use of a single constant shift for all atoms on one side of the interface. We have also performed calculations including self-consistency not only of the dipole but also of the *dipole profile,* i.e., the layer by layer variation of the average point-charge potential. The results for the dipole or band offset of these calculations are in almost perfect agreement with the single-parameter calculation. This provides further strong numerical evidence that a single-parameter calculation describes the macroscopic dielectric response adequately. We will refer to the former (single-parameter) model as the self-consistent-dipole (SCD) model and to the latter (layer shift) as the self-consistent–dipole-profile (SCDP) model.

Our calculations are shown to be in excellent agreement with fully self-consistent LMTO-ASA calculations by Christensen[18] and will also be compared with other calculations and experimental values.

The simplifications brought about by this restricted treatment of self-consistency not only lead to a vast saving in computing time, but, more importantly, to an im-

provement of our understanding of the origin of band offsets and the electrostatics at semiconductor interfaces. The present theory emphasizes the long-range aspect of the potential as the most important degree of freedom for the total energy and the band offsets of the bicrystal. Nevertheless, it considers the band offset, in principle, as an interface property rather than a bulk property since the dipole contribution is, in principle, interface dependent. In practice, this dependence turns out to be small in many cases. This is due to the combination of the screening by a large dielectric constant and the fact that the initial charge transfer and related dipoles themselves are similar for many cases due to their similarity in bonding configuration. While this paper focuses on the (110) interface, we note that similar calculations that we have carried out for the (001) interface of common-anion systems[45] show that the interface-orientation dependence is very small indeed. Larger effects, however, are obtained for non-common-anion systems, and, in particular, for nonisovalent systems.[45,46] For the latter systems, the dipoles depend crucially on the atomic composition at the interface resulting from interdiffusion. Particular compositions with an average bonding configuration similar to the (110) interface will consequently lead to dipoles which are very close to those of the (110) interfaces[4,5,14,45,46] and thus to an apparent interface-orientation independence. It was recently shown that the band offset of CaF_2/Si depends strongly on the interface structure.[47] This is consistent with our theory because of the much smaller dielectric screening in such an ionic system. Also, it has recently been shown that band-offset modification is possible by inserting thin interlayers at the interface.[48]

We therefore conclude that the interface-orientation independence found in a few favorable cases cannot be taken as a valid justification for postulating a "meaningful" absolute reference level in semiconductors. Examples of "absolute" reference levels which have been proposed in the literature are the vacuum level of the atom superposition model[15] or the cation-centered Wigner-Seitz cell model,[17] and the charge-neutrality point.[6–11]

It is important to stress that the present single-parameter SCD approach is based on a first-principles theory. This distinguishes the present calculations from earlier semiempirical self-consistent tight-binding calculations,[12,13] which treat the electrostatics in a similar way but introduce uncertainties due to semiempirical parametrization of the Hamiltonian describing the interactions at the interface. Furthermore, the latter calculations suffer from an arbitrariness in the reference level[49] which is absent from the present work. This work thus establishes a link between the semiempirical self-consistent tight-binding approach,[12,13] and fully self-consistent density-functional calculations.[14–20]

In a separate paper,[46] the preset SCD theory is taken as the basis for an even simpler semiempirical model, the *interface-bond-polarity* (IBP) model. The essential additional feature introduced there is a simple procedure for estimating the initially induced dipole from the polarity of the individual bonds. It allows one to study various interface orientations and configurations very easily and shows that important surface composition effects occur in the case of nonisovalent heterojunctions. Reference 21 contains a preliminary account of the present work and the IBP model.

The paper is organized as follows. Section II describes the theory in a general context. The subsections discuss A, justification of the use of density-functional theory for the band-offset problem; B, reference potential and charge density; C, the restricted freedom variational approach to density-functional theory; D, relation to linear-response theory; E, independence of the self-consistent dipole from the dipole profile; and F, relation between dielectric constants and total energy. Section III fills in the details of the calculation method used in the present work. Section IV presents our results. Section IV A illustrates the single-parameter approach by means of detailed calculated results for a specific example and thus provides numerical evidence for the validity of the theory. It also discusses the calculated dielectric response. Section IV B presents calculated valence-band offsets for a large number of lattice-matched semiconductor (110) interfaces and discusses the results in comparison with other calculations and experiment. Section V summarizes the conclusions of this work.

II. THEORY

A. Introductory considerations

The general framework of the computational procedure followed in this work is density-functional theory (DFT) in the local-density approximation (LDA).[50,51] As is well known, the one-electron eigenvalues or energy bands of the Kohn-Sham[51] equation do not represent quasiparticle excitation energies. Nevertheless, the highest occupied Kohn-Sham eigenvalue is exactly equal to the corresponding quasiparticle excitation energy for the exact exchange-correlation potential.[52] No corresponding statement can be made for the first unoccupied state, because of the possibility of an exchange-correlation discontinuity,[53,54] which has been proposed[55,56] to be the origin of the so-called gap problem in semiconductors. Other authors[57] have proposed that the LDA could be the principal cause for the band-gap underestimates. Therefore we take the usual approach of calculating only the valence-band offsets. The conduction-band offsets can be obtained by adding the experimental values of the energy gaps. In fact, in the LDA, even the top of the valence band is not guaranteed to be exact.[55,56] Still, the self-energy correction calculated by means of the so-called GW approach[55,56] has been shown to be considerably smaller for valence bands than for conduction bands. Furthermore, one expects the corrections to be comparable for the lattice-matched semiconductor pairs considered here and hence to largely cancel out in the band offset. Finally, because the top of the valence band and the dipole are both ground-state properties, it would be inconsistent to treat one beyond LDA without also correcting the other. This justifies our use of the LDA eigenvalues rather than quasiparticle energies for calculating valence-band offsets.

B. Reference level

As mentioned in the Introduction, the band offset can be calculated without introducing an absolute electrostatic reference potential. The only quantities needed are (i) the *difference* of the average potential at the far right and left of the interface, Eq. (1), and (ii) the energies of the band edges *relative* to this average potential in each solid. The first part follows, in principle, from a self-consistent calculation of the heterojunction or bicrystal. The second follows from a calculation of the band structure for the individual solids. The details in the procedure for evaluating the "average" are, in principle, irrelevant. In this work we use the average point-charge potential of the ASA model. Pseudopotential calculations commonly use the volume average of the full electrostatic potential or the pseudopotential.[14–17] Any characteristic energy of the local potential can be used to fix its position with respect to the common, but not explicitly determined, reference level of the whole system. In other words, one only needs a *local* reference level in the two asymptotic regions.

The particular choice for the local reference level made in the present work is tied to our computational method: the LMTO method in the ASA approximation. In this model the potential is spherically averaged within Wigner-Seitz spheres centered about atomic and high-symmetry interstitial sites (in the case of the zinc blende or diamond lattice, the tetrahedral interstitial sites). By construction the only long-range Coulomb effects are those due to the point charges associated with each sphere. The potential from the point charges can be considered as an envelope function for the actual potential, which is obtained by locally replacing the point charge by the actual spherical charge density within each sphere. The *volume-averaged point-charge potential* is chosen as the reference level in the present work. We will refer to this choice as the ASA reference level. The use of this reference level in an absolute sense was proposed previously for absolute deformation potentials[58] and band offsets.[59] A table of band offsets using the ASA reference level has been given in Ref. 15 and, as also shown below, already gives the correct band offsets to within a few tenths of an eV. It forms an essential element in the dielectric midgap energy model.[8]

In order to calculate the cell average of the point-charge potential, one may first average parallel to a given plane (in the present application parallel to the interface) and then average over a period perpendicular to the plane. The planar-average potential has a zig-zag shape consisting of straight line segments which change slope at every lattice plane by an amount $4\pi\sigma$, where σ is the planar-averaged surface charge density of that plane. If several point-charge planes coincide with the same geometrical plane, their potential is simply superposed because of the superposition principle.

Alternatively, one may first calculate the volume average over the Wigner-Seitz spheres,

$$\bar{V}_{\mathbf{R}} = \frac{3q_{\mathbf{R}}}{2s_{\mathbf{R}}} + \sum_{\mathbf{R}'}{}' \frac{q_{\mathbf{R}'}}{|\mathbf{R}-\mathbf{R}'|} , \tag{2a}$$

and finally average over the various spheres with a weight factor proportional to their volume:

$$\bar{V} = \frac{\sum_{\mathbf{R}} \Omega_{\mathbf{R}} \bar{V}_{\mathbf{R}}}{\sum_{\mathbf{R}} \Omega_{\mathbf{R}}} , \tag{2b}$$

where $\Omega_{\mathbf{R}} = 4\pi s_{\mathbf{R}}^3/3$ is the sphere volume. In Eq. (2a), the first term gives the on-site contribution and the second term is the well-known Madelung sum, with $q_{\mathbf{R}}$ the total charge per sphere, i.e., electron plus nuclear charge (units are electronic charges). If all atoms are in equivalent (i.e., symmetry-related) positions, the volume average will automatically be zero when the usual Madelung procedure is used. In general, when the average does not vanish a constant can be added in order to make $\bar{V} = 0$.

Note that the above-defined reference level is a bulk property. It is essential in the above that the potential is chosen to be periodic as well as the charge density. This automatically guarantees that there are no macroscopic electric fields and fixes the potential to within a constant. The cell average is then well defined and can be chosen equal to zero. In the present work, these considerations apply to the point-charge contribution to the potential as well as the full ASA potential.

It is useful and instructive to describe the heterojunction in terms of its changes from a reference model[60] based on the bulk charge density, or, as in the present ASA context, a point-charge distribution. The latter must be chosen such that the reference potential, i.e., the bulk potentials with a chosen lineup, follow from it through Poisson's equation. One can then describe the charge density and potential of the heterojunction by means of their changes from the reference model with the changes themselves related by Poisson's equation. In general, the reference charge density does not consist solely of the bulk charge densities of the two solids, because "cutting" the solids in an arbitrary way and "gluing" the two half-solids together with frozen charge densities may lead to a macroscopic electric field as well as a dipole shift at the interface. In order to avoid this, one must add a compensating surface charge density for the two half-solids. The latter can easily be chosen such that the electric field emerging in the vacuum region as a result of breaking the periodicity of the solid at the surface is compensated. This requirement fixes the total charge of the surface compensating charge density. Furthermore, the distribution of this charge determines the surface dipole, i.e., average internal potential with respect to the vacuum potential. The latter fixes the initial lineup of the reference model. In particular, the surface dipole can be chosen to vanish, whereby the initial lineup corresponds to the bulk reference lineup discussed above. Note that no self-consistent calculation of the surface is necessary as one only seeks a charge density and potential which satisfy Poisson's equation but not necessarily Schrödinger's equation. For the point-charge densities and potentials of the ASA, one may take the compensating surface charge density of the reference model to be a planar-averaged point-charge distribution in the vacuum

positioned such that the surface point-charge dipole is zero and the initial lineup corresponds to zero dipole. Unlike the reference potential, which can be chosen independently of the surface, the corresponding charge density is surface dependent. The reference-model concept as described above was used in a calculation of the Schottky barrier for $NiSi_2/Si$.[61] The "cut-and-glue" model is particularly appropriate if the boundary is chosen in a physically meaningful way, i.e., along regions of low electron density. The boundaries of the ASA spheres appear to satisfy this requirement very well as may be seen in the contour plots of the charge density in Ref. 61.

C. Restricted variational freedom approach

The DFT equations can be considered as a variational approach for the total energy in terms of the effective Kohn-Sham potential as a basic variable. In the present work, severe restrictions are imposed on the effective one-electron potential. In the first place, we restrict the discussion to ASA potentials. This approximation assumes that space can be filled with Wigner-Seitz spheres. This is not strictly true and therefore we start from the approximate ASA total-energy functional.

1. ASA functional

The ASA functional is defined by the following procedure.

(i) Solve the Kohn-Sham Schrödinger equation,

$$[-\tfrac{1}{2}\nabla^2+v_{\rm in}(\mathbf{r})]\psi_k(\mathbf{r})=\varepsilon_k\psi_k(\mathbf{r}) \;, \tag{3}$$

for $v_{\rm in}$ the input potential restricted to the ASA form:

$$v_{\rm in}(\mathbf{r})=\sum_{\mathbf{R}} v_{\mathbf{R}}^{\rm in}(r) \;. \tag{4}$$

(ii) Construct a spherically averaged trial electron density from the occupied eigenfunctions:

$$n_{\mathbf{R}}(r)=\frac{1}{4\pi}\int\sum_{k}^{\rm occ}|\psi_k(\mathbf{r})|^2 d\hat{\mathbf{r}} \;. \tag{5}$$

(iii) Evaluate the total energy functional as a function of this trial density:

$$E_{\rm tot}=T+U+U_M \;. \tag{6}$$

Here the kinetic energy T of the model-independent electron system is given by

$$T=\sum_{k}^{\rm occ}\varepsilon_k-\sum_{\mathbf{R}}\int_{s_{\mathbf{R}}} v_{\mathbf{R}}^{\rm in}(r)n_{\mathbf{R}}(r)d^3r \;. \tag{7}$$

The intrasphere electrostatic and exchange-correlation contributions are given by

$$U=\sum_{\mathbf{R}}\int_{s_{\mathbf{R}}} d^3r\, n_{\mathbf{R}}(r)\left[\frac{1}{2}\int_{s_{\mathbf{R}}} d^3r'\frac{n_{\mathbf{R}}(r')}{|\mathbf{r}-\mathbf{r}'|}-\frac{Z_{\mathbf{R}}}{r}+\varepsilon_{\rm xc}[n_{\mathbf{R}}(r)]\right] , \tag{8}$$

with $Z_{\mathbf{R}}$ the nuclear charge at site $\mathbf{R}$, and $\varepsilon_{\rm xc}$ the exchange-correlation energy per electron. Finally, the intersphere contribution is given by the point-charge energy excluding the self-interaction, usually called the Madelung energy:

$$U_M=\tfrac{1}{2}\sum_{\mathbf{R}}\sum_{\mathbf{R}'}{}'\frac{q_{\mathbf{R}}q_{\mathbf{R}'}}{|\mathbf{R}-\mathbf{R}'|} \;. \tag{9}$$

Minimizing the total energy is now equivalent to self-consistency of the ASA potentials:

$$v_{\mathbf{R}}^{\rm out}(r)\equiv\int_{s_{\mathbf{R}}}\frac{n_{\mathbf{R}}(r')}{|\mathbf{r}-\mathbf{r}'|}d^3r'-\frac{Z_{\mathbf{R}}}{r}+\mu_{\rm xc}[n_{\mathbf{R}}(r)]+\sum_{\mathbf{R}'}{}'\frac{q_{\mathbf{R}'}}{|\mathbf{R}-\mathbf{R}'|}=v_{\mathbf{R}}^{\rm in}(r) \;. \tag{10}$$

Here, the exchange-correlation potential $\mu_{\rm xc}[n]=\partial[n\varepsilon_{\rm xc}[n]]/\partial n$.

Note that the ASA total-energy functional is different from the true Kohn-Sham functional (both considered as a functional of the potential) because in the former the *charge density* has been spherically averaged. Alternatively, one might have kept a nonspheridized charge density even in conjunction with a spherical ASA potential. In that case, the ASA self-consistent potential only approximately minimizes the true total-energy functional. In the present formulation, on the other hand, the *approximate* ASA functional is minimized *exactly*.

2. Frozen-shape approximation

Additional restrictions can be imposed on the trial potential. In the present work, the radial dependence of the potential wells inside each Wigner-Seitz sphere will be taken to be the same as in the self-consistently calculated bulk solids except for a constant shift per sphere. This constitutes the so-called *frozen-shape* approximation, previously used by Kollar and Andersen[62] in a study of the heat of formation of alloys. This line of work is an extension of the frozen potential approach (without constant shifts[63–65]), which itself is a generalization of the so-called force theorem,[66] originally derived for infinitesimal displacements.

It is possible to replace the ASA total-energy functional, Eqs. (3)–(9), by a new approximate functional which is exactly minimized by the self-consistency of the restricted parameter space for the trial potential. This leads to closed simplified expressions for energy differences such as the heat of formation, mentioned above. A similar approach has recently been used by us to calculate the energy of formation of superlattices.[67] It is a perfectly valid procedure, however, to search for the minimum only within a restricted parameter space and still to evaluate the complete functional with the approximate solution for the minimum. In fact, in the present paper there is no need to write the approximate functionals explicitly because the total energy is not the primary property of interest. Nevertheless, it is important to realize that the SCD or SCDP calculations used here to determine the di-

pole correspond to a variational calculation of the total energy.

3. *SCDP model*

In the SCDP model we not only restrict the degrees of freedom to a constant shift per atomic sphere but, in addition, average over all sphere types lying in the same geometrical lattice plane. In the following we refer to the region encompassing all the spheres whose centers lie in the same geometrical plane as a *layer.* The justification for this additional approximation is that we wish to focus on the planar average of the potential parallel to the interface: the so-called dipole profile. The lateral degrees of freedom in the potential are thus intentionally filtered out in addition to the radial degrees of freedom already removed by the frozen-shape approximation. One may perform this filtering also on the charge density, or, rather on the point-charge distribution. The reason for this is that the lateral variables in Poisson's equation are independent of the perpendicular degree of freedom. These approximations simplify the electrostatics considerably as it becomes purely one dimensional and discrete. The planar-averaged point-charge potential is a piecewise linear function as already discussed in Sec. II B. In addition, we here only need its value at lattice planes and thus the charge density as well as the potential reduce to discrete shifts per atomic layer. Note that we have first spherically averaged (corresponding to the ASA), then volume averaged over each sphere (corresponding to the frozen-shape approximation), and finally laterally averaged over the sphere types within the same layer. The present procedure not only is a constant shift approach but also a purely electrostatic approach; i.e., the small exchange-correlation contribution to the potential is rigidly kept frozen. Slightly different procedures could be taken for the contraction of the full output potential to a frozen-shape potential, namely by performing the averages in a different order. For example, one might first consider the full point-charge potential, which is not constant over the spheres, and only in the final step make the frozen-shape approximation of averaging over the spheres. These different alternatives should have minor effects on the results.

An example of a dipole profile is shown in Fig. 1. This figure illustrates the method by means of a calculation for the ZnSe/AlAs(110) interface. The atomic layers parallel to the (110) interface are neutral in the bulk solids because the 2D unit cell per layer contains effectively one primitive 3D unit cell, i.e., both the cation and the anion, and the two types of empty spheres centered at the tetrahedral intersitial sites. The average point-charge potential per layer in the bulk is thus zero on all the layers and in the starting potential for the heterojunction the latter are simply lined up for both semiconductors, i.e., $D_{\rm in}^{1}=0$. There is no need in this case to introduce a surface compensating charge. After solving the Schrödinger equation for the heterojunction, the layer-averaged point charges q_n^1 shown by the shaded histogram in Fig. 1 are obtained, where n indicates the layer number. Solving the 1D Poisson equation, now reduced

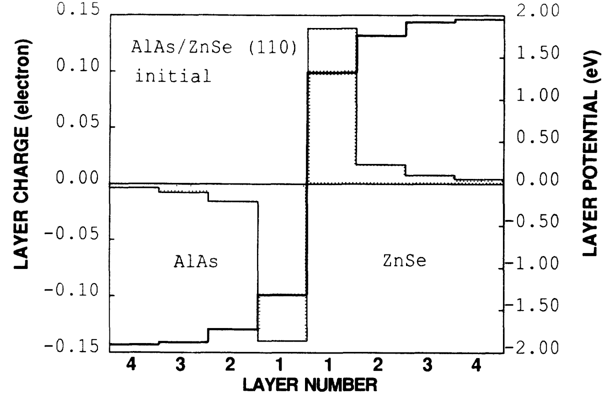

FIG. 1. Initially induced layer charge (shaded) and associated electrostatic potential at the center of each layer (bold line) for ZnSe/AlAs (110) starting from the ASA lineup. Each layer contains a cation, an anion, and two empty spheres, and is neutral in the bulk.

to a finite-difference equation, because of the planar δ-function nature of the charge density, produces the output layer-averaged point-charge potentials V_n^1, shown in Fig. 1 as the bold line. The output dipole $D_{\rm out}^{1}$ is the difference between the asymptotic values of this layer potential on either side of the interface. Clearly, the starting layer potential which vanishes on all the layers is not self-consistent in this case because the output potential shifts are large on each layer. In the present case, the changes in charge and potential from the reference model as discussed in Sec. II B equal the charges and potentials themselves. The layer point-charge potential V_n must now be adjusted to self-consistency. The self-consistent results will be discussed in Sec. IV.

4. *SCD model*

In the SCD model the potential is restricted even further: a single shift of the potential per semiconductor half-space is kept as the only degree of freedom. Clearly, by definition the dipole and thus the band offset only depend on this shift, once the charge density has been determined self-consistently. That one may actually restrict the variational search to this single-parameter space is not so evident *a priori* but will be discussed below. Clearly, a single-step dipole profile as input does not result in a single-step output profile, but the output dipole, defined as in Eq. (1), is well defined. It is given by

$$D_{\rm out}=\frac{4\pi}{\Omega}\sum_{n} q_n z_n \ , \tag{11}$$

where Ω is the 2D unit cell area, and z_n are the positions of the layers.

In this single-parameter model, self-consistency is most easily obtained by means of a graphical procedure illustrated in Fig. 2 for the example of ZnSe/AlAs(110). One simply performs a few calculations of $D_{\rm out}$ as a function

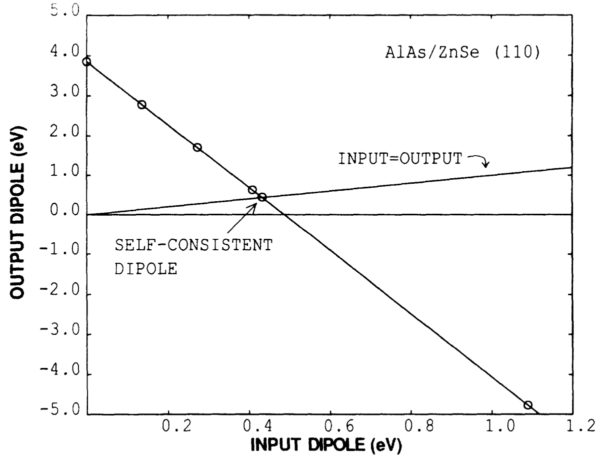

FIG. 2. Graphical procedure for finding the self-consistent dipole. A single-step dipole profile with a given input dipole is used as input, and the output dipole is the result of a single iteration of Schrödinger's and Poisson's equation. The zero-input dipole corresponds to the ASA lineup. The self-consistent solution corresponds to the intersection with the line "input=output." The circles indicate calculated points, the straight line is an interpolation. Note the different scales for input and output.

of D_{in} and looks for the intersection with the line $D_{\text{out}}=D_{\text{in}}$. An important result, demonstrated by Fig. 2, is that the curve $D_{\text{out}}(D_{\text{in}})$ is quite linear over a wide range around the self-consistent solution D_{SCF}. Consequently, only two calculations are sufficient to obtain the curve in the relevant region. The self-consistent solution is obtained from the value D^1_{out} in one point D^1_{in}, e.g., $D^1_{\text{in}}=0$ and the slope D':

$$D^1_{\text{out}}=D_{\text{SCF}}+D'(D^1_{\text{in}}-D_{\text{SCF}}) ,$$

from which it follows that

$$D_{\text{SCF}}=D^1_{\text{in}}+\frac{D^1_{\text{out}}-D^1_{\text{in}}}{1-D'} . \tag{12}$$

In principle, one should take the slope in the self-consistent point, but in practice it does not matter which point is chosen as long as one is within the linear range. In the following section, we relate this approach to standard linear-response theory.

D. Linear-response theory

In standard linear-response theory, one starts from a given system in equilibrium and asks for the new equilibrium situation when a small perturbation is added. In the present context, this means that one assumes that the self-consistent solution $\mathbf{V}_{\text{SCF}}$ has been found. In this subsection, $\mathbf{V}$ is the one-electron potential of the system and depending on the level of approximation it may stand for the dipole D, the layer-averaged point-charge potential V_n, the sphere-volume-averaged point-charge potential at each site $V_{\mathbf{R}}$, the spherical-averaged potential $v_{\mathbf{R}}(r)$, or the full $\mathbf{r}$-dependent potential $v(\mathbf{r})$. In the language of signal processing $\mathbf{V}_{\text{SCF}}$ defines the "working point." Now, one adds a small perturbation, called the bare perturbation $\Delta\mathbf{V}_{\text{bare}}$. We use a Δ notation to stress that this is the "small signal" on top of the "working point." A single iteration of the Schrödinger equation and the Poisson equation is illustrated diagrammatically in Fig. 3. The solution of Schrödinger's equation, after filling the one-electron states according to Fermi-Dirac statistics, provides the induced electron density,

$$\Delta\mathbf{n}^1_{\text{ind}}=\chi^0\Delta\mathbf{V}_{\text{bare}} . \tag{13}$$

The full charge-density change $\Delta n^1(\mathbf{r})$ can, if necessary, be contracted to a spherically averaged $\Delta n^1_{\mathbf{R}}(r)$, a change in the total charge per sphere $\Delta q^1_{\mathbf{R}}$ or per layer Δq^1_n or the dipole moment $\Delta P^1=\Omega^{-1}\sum_n \Delta\hat{q}_n z_n$ to the desired level of approximation. The quantity χ^0 is called the bare susceptibility. It is a second-rank tensorlike quantity. Depending on the approximation level it can stand for a nonlocal operator, a matrix, or a scalar. In the most general case, Eq. (13) corresponds to a convolution integral of $\chi^0(\mathbf{r},\mathbf{r}')$ with $\Delta v_{\text{bare}}(\mathbf{r})$. The induced charge density gives rise to an induced potential,

$$\Delta\mathbf{V}^1_{\text{ind}}=u\;\Delta\mathbf{n}^1_{\text{ind}} , \tag{14}$$

by means of the Poisson equation and the local-density exchange-correlation potential which is included in the most general formulation. In the single-parameter case $u=4\pi$, whereas in general it is a tensorlike quantity such as χ^0. If so desired, the fully $\mathbf{r}$-dependent potential can again be contracted to the desired level of approximation. This induced potential is now added to the bare perturbation and the new equilibrium situation implies a self-consistently screened perturbation given by

$$\Delta\mathbf{V}_{\text{screened}}=\Delta\mathbf{V}_{\text{bare}}+u\chi^0\Delta\mathbf{V}_{\text{screened}} . \tag{15}$$

In other words,

$$\Delta\mathbf{V}_{\text{screened}}=(1-u\chi^0)^{-1}\Delta\mathbf{V}_{\text{bare}} \tag{16}$$

$$\equiv\epsilon^{-1}\Delta\mathbf{V}_{\text{bare}} . \tag{17}$$

The last equation is a definition of the inverse dielectric function ϵ^{-1}, which leads to the relation

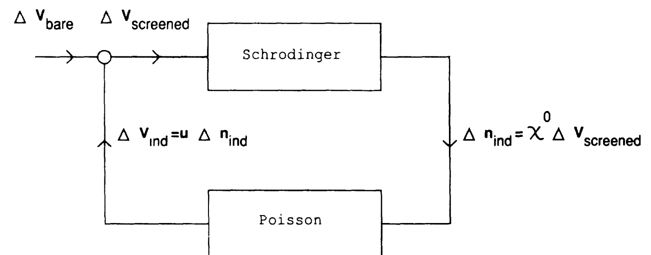

FIG. 3. Schematic diagram of a single iteration of Schrödinger's and Poisson's equation. The latter may include exchange and correlation contributions as well.

$$\epsilon=1-u\chi^0 . \tag{18}$$

This is the well-known random-phase approximation (RPA) result. Often one also introduces the self-consistently induced potential and the screened susceptibility by

$$\Delta\mathbf{V}_{\text{ind}}\equiv\Delta\mathbf{V}_{\text{screened}}-\Delta\mathbf{V}_{\text{bare}} \tag{19}$$

$$=u\chi^0\Delta\mathbf{V}_{\text{screened}} \tag{20}$$

$$\equiv u\chi\Delta\mathbf{V}_{\text{bare}} , \tag{21}$$

from which one finds

$$\chi=\chi^0(1-u\chi^0)^{-1} . \tag{22}$$

Finally, one has

$$\epsilon^{-1}=1+u\chi . \tag{23}$$

Because the perturbations are within the linear-response range, one has

$$u\chi^0=\frac{\Delta\mathbf{V}_{\text{ind}}}{\Delta\mathbf{V}_{\text{screened}}}=\frac{\Delta\mathbf{V}^1_{\text{ind}}}{\Delta\mathbf{V}_{\text{bare}}}=\frac{\delta\mathbf{V}_{\text{out}}}{\delta\mathbf{V}_{\text{in}}} , \tag{24}$$

where a functional derivative notation is used for generality, and the subscripts, out and in, refer to input of Schrödinger's equation and output of Poisson's equation, i.e., one iteration cycle. In the single-parameter model, it reduces to the slope D', discussed in the preceding subsection. In the case of discrete parameters, such as the sphere or layer potential shifts, it reduces to the Jacobian matrix $\partial V_i^{\text{out}}/\partial V_j^{\text{in}}$, where i,j indicate the discrete indices such as sphere site $\mathbf{R}$ or layer number n.

We have now established the connection of the self-consistent calculations to standard linear-response theory, and, in particular we have identified the slope of the $D_{\text{out}}(D_{\text{in}})$ curve in the single-parameter model as

$$D'=4\pi\chi^0=1-\epsilon . \tag{25}$$

In the following subsection we discuss which dielectric constant is relevant in this context.

Note that the calculation at the end of Sec. II C corresponds to determining the working point, which in the present case is not known *a priori*. In fact, one is interested in the system without external perturbation, and the above connection with linear-response theory is only used to establish the physical meaning of the output-input relation of each iteration.

E. Independence of the dipole profile

The preceding subsections [see Eqs. (12) and (25)] lead to the conclusion that within the SCD model the self-consistent value for the point-charge potential dipole is obtained from

$$D_{\text{SCF}}=D^1_{\text{in}}+\frac{D^1_{\text{out}}-D^1_{\text{in}}}{\epsilon} . \tag{26}$$

As this dipole refers to the asymptotic values of the potential [Eq. (1)], it is clearly the *macroscopic* dielectric constant of the heterojunction region (to be specified more clearly below) which is relevant. Furthermore, we take the atomic positions to be frozen within the Born-Oppenheimer approximation so that no ionic displacements contribute to the screening. Also, the perturbation is static. Thus the relevant frequency range is just above the reststrahlen frequency, i.e., low with respect to electronic energies, but high with respect to ionic motion frequencies.

Now, we will argue that Eq. (26) is valid, at least approximately, beyond the SCD model. At the same time, we will attempt to specify the macroscopic dielectric constant of the heterojunction more precisely. Specifically, we want to show that the dipole part of a perturbation will be screened by the macroscopic dielectric constant independently of the detailed shape of the dipole profile (within certain restrictions, to be discussed below).

For simplicity, we first consider a perturbation to a perfect crystal rather than a heterojunction. The perturbation is assumed to contain a step part D plus arbitrary modulations in the vicinity of the interface. In other words, it is completely arbitrary in the interface region but approaches a constant value on the far left of the interface and another constant value on the far right. This problem has been discussed by Resta and Kunc.[68] These authors have shown that the resulting screened dipole is, in general, *not* given by D/ϵ but includes local-field corrections. One can easily understand the origin of these terms in direct space. A point charge q placed at a general nonsymmetrical position in the solid will induce not only a monopole but also a dipole and higher-order screening charge-density components. For example, it might draw more charge from the side of the closest atom or bond. However, the leading term is a monopole, i.e., a net charge reducing the effective point charge seen at large distance to q/ϵ. Next, consider a dipole built up of two point charges at a distance d. At large distance, each charge is reduced by a factor ϵ and thus the leading term contains the dipole D/ϵ. In addition, however, the dipole components in the microscopically induced charge density in general lead to a net dipole potential, the so-called local-field contribution. It is also clear, however, that if the dipole is placed in a mirror plane of the crystal perpendicular to itself, the total local-field contribution will vanish by symmetry. Within the ASA model used here, this is always the case because only point charges centered on tetrahedral sites are considered. In the present case we are dealing with a layer of dipoles rather than a single dipole. This only simplifies the discussion because the electrostatics becomes effectively one dimensional. The same result holds: if the dipole layer is placed in a symmetry plane, the dipole potential step will be screened by the macroscopic dielectric constant. Also, it is clear that modulations of the dipole step will only affect higher-order terms and not the dipole itself, provided they do not break the symmetry required to make the net microscopic or local-field contribution vanish.

For the heterojunction, a corresponding exact result cannot be proven because the symmetry is broken from the start. The distinction between microscopic or local-field effects in the screening and macroscopic screening is only well defined with respect to a crystalline solid. Also,

it is obvious that the "macroscopic" dielectric constant of the interface region depends to some extent on how the region is chosen, in other words how much it extends in each material. Furthermore, the local electronic structure near a heterojunction, and consequently the dielectric properties, are in principle modified. However, it turns out that the changes (e.g., in the local densities of states) are generally small. Thus, one expects the screening properties to be some kind of average of those for the two semiconductors. Also, all the perturbations we consider have about an equal extent in each semiconductor. The same is true for the screening lengths. Consequently, one may expect that Eq. (26) still holds approximately independently of the details of the dipole profile, as long as the above-mentioned conditions are fulfilled. The dielectric constant should be an average dielectric constant of the two materials representative of the interface region, chosen large enough to encompass all the screening charge and having about equal extent in each of the semiconductors. In practice, our calculations show that this region extends only over a few atomic layers. This is already large enough to produce "macroscopic" screening.

If we consider the semiconductors to be classical dielectrics with macroscopic dielectric constants ϵ_A and ϵ_B, the screening of a dipole field can easily be carried out by means of the image-potential method. Assuming the dipole is produced by two oppositely charged sheets (with surface charge density σ) a distance d apart and placed at a distance d_A from the interface into semiconductor A and d_B into semiconductor B, one finds that the dipole $D_{\text{ext}}=4\pi\sigma d$ is reduced to

$$D_{\text{scr}}=4\pi\sigma(d_A/\epsilon_A+d_B/\epsilon_B) . \tag{27}$$

Thus the effective dielectric constant of the heterojunction is given by

$$(d_A+d_B)/\bar{\epsilon}=(d_A/\epsilon_A+d_B/\epsilon_B) . \tag{28}$$

For equal (or nearly equal) distances $d_A \approx d_B$ this reduces to the harmonic average

$$\bar{\epsilon}^{-1}\approx\tfrac{1}{2}(\epsilon_A^{-1}+\epsilon_B^{-1}) . \tag{29}$$

The same result can also be obtained by realizing that each part of the heterojunction can be represented by an effective capacitance. We thus have a series connection of capacitances and as the surface area is the same for all of them, one immediately obtains Eqs. (28) and (29). The above considerations for the simplest dipole profile corresponding to two sheets of charge can easily be generalized to more general dipole profiles. Clearly, the result is independent of the details of the profile as long as the change in charge density from the reference charge density producing the dipole is essentially antisymmetric about the interface. From the initial dipole profile shown in Fig. 1 and from similar results for the other heterojunctions we have calculated, we found that this is indeed the case. As a result, we expect the effective macroscopic dielectric constant of the heterojunction to be given approximately by the harmonic average of the dielectric constants of the semiconductors involved.

F. Dielectric constants and total energy

In practice, a self-consistent DFT calculation, with or without restrictions on the degrees of freedom, implies a calculation of the dielectric response. It is thus important to check how well the restricted degree of freedom method describes the dielectric response. In the strictest sense, we cannot really check this for the heterojunctions because it is, in principle, not uniquely defined as discussed above. However, we have recently used essentially the same approach to calculate the macroscopic dielectric response function of pure semiconductors[69] and obtained very good agreement with other calculations. However, we also found that the LDA itself leads to an overestimate of the macroscopic dielectric constant by $\sim 10-30\,\%$ depending on the semiconductor. In a recent paper, Hybertsen and Louie have reached similar conclusions about the LDA errors on the macroscopic dielectric constant,[70] although they took a completely different approach.

To obtain some understanding for the validity of the single-parameter approximation for the calculation of the dielectric constant, it is instructive to return to the total-energy expression. In the notation developed in Sec. II D, it is easily shown that

$$\frac{\delta E_{\text{tot}}}{\delta \mathbf{V}_{\text{in}}}=\chi^0(\mathbf{V}_{\text{out}}-\mathbf{V}_{\text{in}}) , \tag{30}$$

and from Eqs. (24) and (18)

$$\frac{\delta^2 E_{\text{tot}}}{\delta \mathbf{V}_{\text{in}}\delta \mathbf{V}'_{\text{in}}}=-\chi^0(1-u\chi^0)=-\chi^0\epsilon . \tag{31}$$

This means that the curvature of the total energy in the abstract parameter space of the various degrees of freedom is proportional to the corresponding dielectric response function. A schematic and hypothetical contour plot of the total energy in a two-parameter space is given in Fig. 4. One may think of the parameter V_1 as the dipole and V_2 the local potential distribution near the interface to be added to a single-step dipole profile in order to obtain the actual dipole profile. The long-range or macroscopic dielectric function is much larger than the short-range response function,[71] and thus the total energy varies most rapidly for the long-range degree of freedom. This makes the contour elongated along the V_2 axis. Also, the off-diagonal elements of the dielectric matrix in this parameter space are small. Physically, this means that long-range screening is essentially independent of short-range screening, which is a plausible assumption. As a result, the contour shape in Fig. 4 lies essentially perpendicular to the coordinate axes. In this situation, even if one is not at the minimum for V_2, the minimum as a function of V_1 should give a value of V_1 close to that of the true minimum.

The numerical results, to be presented in Sec. IV, give support to the tentative and qualitative picture of the total-energy function sketched above. Indeed, the single-parameter (SCD) calculations will be shown to be in good agreement with the multiparameter (SCDP) calculations and with fully self-consistent ASA calcula-

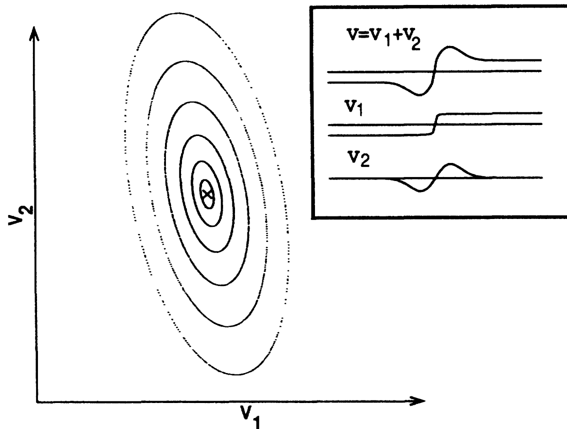

FIG. 4. Schematic qualitative contour plot of the total energy as a function of the long-range (V_1) and short-range (V_2) potential degrees of freedom. Schematics of V_1 and V_2 are shown in the inset. The minimum is indicated by the cross. The elongated shape indicates the smaller curvature (i.e., dielectric constant) of the total energy as a function of the short-range components compared to the long-range components. The orientation of the principal axis being nearly parallel to the axes indicates the near independence of the long-range and short-range components.

tions[18] which involve even a much larger number of degrees of freedom. The macroscopic dielectric constants themselves obtained by means of the SCD calculation will be shown to be in fair agreement with the harmonic average of the experimental dielectric constants of the two semiconductors, at least, to within the uncertainties of the LDA.

III. COMPUTATIONAL METHOD

The basic elements of the computational procedure have already been described in the preceding section. They are local-density-functional theory, a restricted variational approach for the self-consistency, and the LMTO-ASA method for solving Schrödinger's equation. Here, we provide some further details on the computational procedure.

In order to solve Schrödinger's equation for the heterojunction, we make use of a supercell model. This introduces an artificial periodicity into the system and the supercells must be chosen sufficiently large to assure convergence to the true asymptotic values. Alternatively, one might use a recently proposed tight-binding LMTO Green's-function technique.[72] The latter deals with truly semi-infinite systems and is very useful for detailed investigations of the nature of electronic states near an interface, especially if they are very extended. For the present purpose, only average features of the electronic structure are relevant and the supercell approach was preferred for its simplicity.

The supercells used for the (110) interface consist of seven layers of each material, where each layer contains both a cation and an anion and two types of empty spheres at the tetrahedral interstitial sites. This supercell is referred to as 7+7 and contains 56 spheres, e.g., $(\mathrm{GaAs}EE')_7(\mathrm{AlAs}EE')_7$, where E,E' indicate the empty spheres. This size was found to be adequate, as indicated by the fact that at self-consistency, the charge distribution took on the appropriate bulk values in the central layers of each half of the supercell. In some cases, additional calculations for a (9+9)-cell (72 spheres) were carried out and in each case the results were in excellent agreement with those for the smaller supercells.

In this work, we have only considered nearly lattice-matched semiconductor heterojunctions. A common lattice constant was chosen for each group of nearly lattice-matched semiconductors, in effect making them perfectly matching. Strain effects, due to nonperfect matching, are neglected, but could easily be incorporated, if necessary.

The supercells are used to determine the dipole and, because this is an average quantity, the calculations were performed strictly within ASA, i.e., without the combined correction term.[44] The tight-binding representation is used to calculate the structure constants because this is a faster procedure for the large supercells than the Ewald procedure required for the unscreened structure constants. The calculations are performed by subsequent transformation to the nearly orthogonal representation and including third-order corrections to the eigenvalues by means of perturbation theory. The bulk potential and potential parameters which give the starting point for the supercell calculations were determined using the standard primitive unit cell of the sphalerite structure and a self-consistent calculation also without the combined correction. Single-panel calculations were used in all cases. The shallow core *d* states of Ge, Ga, Sn, and In were treated as frozen core states, while for Cu, Zn, Hg, and Cd, the *d* states were included as band states in the valence-band panel. A single special **k** point[73,74] in the irreducible part of the Brillouin zone (BZ) was found to be adequate in view of the large supercells (small BZ) involved and considering the approximate and average nature of the quantities we are calculating. This was confirmed in some specific cases by increasing the number of **k** points to four in the surface BZ.

As the position of the valence-band maximum with respect to the ASA reference turns out to be particularly sensitive to various details in the calculation, the combined correction term was included for this purpose. Also, it was found for CuBr that using the potential of a two-panel self-consistent calculation, with the very deep Br 4*s* band in a separate panel, shifts the top of the valence band down by 0.05 eV. One may expect some compensation in the dipole if the latter were also calculated with two panels; however, this point was not fully investigated. Finally, in order to determine the position of the valence-band edge with respect to the ASA reference, we have placed the linearization energy $\varepsilon_{\nu l}$ near the top of the valence band for all angular momenta in order to minimize errors due to the linearization. The effects of the above refinements were not included in the results reported in the earlier version of our work.[21]

The calculations are scalar relativistic, i.e., they contain all relativistic effects except spin-orbit coupling. The

latter splits the top of the valence band and a correction for this splitting can easily be added *a posteriori*. Experimental spin-orbit splittings[75] were used where available and calculated separately for the other cases (CuBr,SiC,AlN,AlP).

For later comparisons of the results it is important to point out here that our calculations differ from Christensen's LMTO calculations for semiconductor heterojunctions[18] in several respects. Christensen used two-panel calculations and included the combined correction term in all cases including the supercell calculations. Also, for the purpose of calculating the position of the valence bands with respect to the ASA potentials, Christensen used a slightly different procedure for treating the *d* bands than ours. For II-VI compounds and for Ga and In compounds, he performed two calculations: one with ε_{vd} at the center of gavity of the lower *d* band and one with ε_{vd} up in the conduction band. He then took the average of both results. This procedure is not too sensitive to the exact position of the upper ε_{vd} as long as no *d* band occurs at the energy of interest. It is thus expected to give good agreement with our procedure. Nevertheless, the simpler procedure adopted by us seems preferable and more natural within the context of linear methods.

As a result of these differences in the procedural details, the ASA reference level band offsets presented here show significant differences (of the order of 0.2 eV) with the ones previously published in Refs. 15 and 8. As a further possible reason for this discrepancy, we mention the fact that an accurate determination of the position of the bands with respect to the ASA reference requires extremely well-converged calculations. The small differences in initial lineup, however, are compensated by corresponding changes in the dipole of the heterojunction. The band offsets only involve small relative energy differences and these are much less sensitive than the large energies of the valence band with respect to the ASA reference. As a result, we will see in Sec. IV that the final band offsets are in very good agreement with Christensen's calculations. The additional approximations for the supercells in our work (no combined correction and single panel) largely cancel in the differences giving the band offsets.

As discussed extensively in Sec. II, the self-consistency treatment is dramatically simplified in the present work. This, in fact, is the central theme of this paper. In addition to the added insights gained from the simplifications, they also lead to a vast reduction in the required computing time. In the SCD model, only a few band-structure calculations for the supercell are needed using the graphical procedure to determine self-consistency. Even for the multiparameter SCDP model, the computing time savings with respect to standard ASA calculations are substantial. This is mainly due to the small number of degrees of freedom. Very efficient schemes, such as Broyden's[76] Jacobian update technique, can be used to iterate the limited set of parameters to self-consistency in a few iterations. Typically, only 5–8 iterations are necessary to achieve convergence to within 1 mRy. Also, because of the approximate nature of the calculation (frozen potential and layer averaging) a smaller number of **k** points is required. The net result is a reduction in computing time by a factor of 10 or larger.

IV. RESULTS

A. Illustration of the theory by numerical results

In this section, we illustrate some aspects of the theory presented in Sec. II by means of numerical results. First we discuss the SCD model. The result of a typical SCD calculation has already been shown in Fig. 2. This figure shows that the output-input curve for the dipole is linear over a very wide range. Entirely similar behavior was found in all cases considered in this paper. This justifies our use of the linear-response theory described in Sec. II D. In order to test that the SCD method also provides the dielectric constant itself, we compare the calculated macroscopic dielectric constant [i.e., $1-D'$ with D' being the slope of the line $D_{\text{out}}(D_{\text{in}})$] with the appropriate experimental dielectric constant of the heterojunctions. For the latter, we choose the harmonic average of the individual semiconductor's dielectric constants, for reasons explained in Sec. II E. The result is shown in Fig. 5. Clearly, a very good correlation is obtained. However, the calculations generally overestimate the dielectric constant. As has been shown elsewhere, this can be ascribed essentially to the LDA approximation for exchange and correlation[69] which is known to lead to an underestimate of the band gap. Although it is by no means obvious that this should also lead to an overestimate of the dielectric constant, because the matrix elements might play an im-

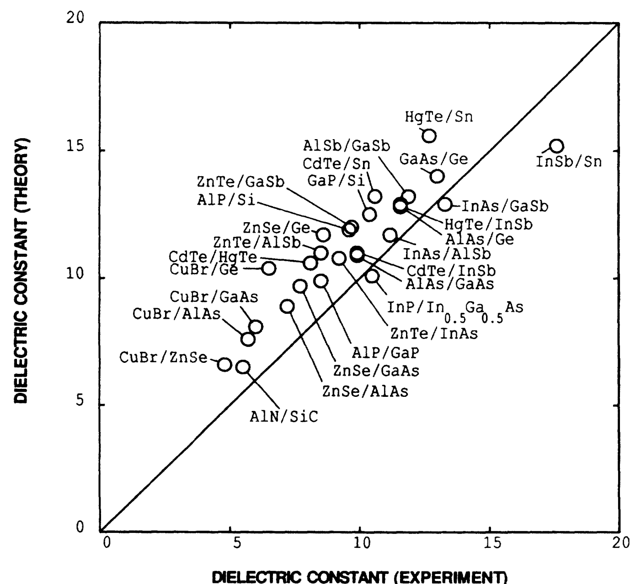

FIG. 5. Correlation between theoretical ($1-D'$, with D' being the slope of the output dipole vs the input dipole curve) and experimental macroscopic dielectric constant (harmonic average of the dielectric constants of the two semiconductors). The experimental values are taken from Ref. 3.

portant compensating role, we found that adjusting the potential parameters so as to correct the band gap improved the dielectric constants considerably. This indicates that the primary reason for the discrepancy is indeed the LDA. Note that because the self-consistent dipoles are of the order of a few tenths of an eV, an overestimate of the dielectric constant by ~10% causes errors in the dipole or band offset only of the order of a few hundredths of an eV.

Next, we consider results of the SCDP model. Figure 6 shows the self-consistently calculated dipole profile for the same example as used previously. This figure should be compared to the non-self-consistent output of the first iteration, which was shown in Fig. 1. The most striking differences are the changes in magnitudes. This is due to the dielectric screening of the initially induced dipole. The self-consistent dipole, obtained from the SCDP calculation, is 0.43 eV, in perfect agreement with the result of the SCD calculation. Again, this is not a fortuitously favorable example but the universal behavior. As already pointed out above, the LDA itself introduces errors of the order of 10% in the dielectric constant and thus of the order of 0.01–0.05 eV in the dipole. The deviation between the SCDP and SCD results for the dipole is at most 0.02 eV. This gives very strong support to our statement that the macroscopic screening within the LDA is described adequately by the single-parameter variational approach.

The results of the SCD and SCDP calculations are compared in more detail in Fig. 7. The latter compares the self-consistent dipole profile (i.e., the result from the SCDP calculation) with the output dipole profile of a single iteration, in which a single-step dipole profile with the same dipole is used as input. Although the dipole profiles differ, they give exactly the same asymptotic values. This shows explicitly that the output dipole is independent of the profile of the input dipole.

Although the band offset only depends on the dipole and not on the dipole profile, it is instructive to consider the dipole profile in some detail. Figure 7 shows that the dipole profile is smoother in the SCDP calculation than in the SCD calculation. This is expected because in the SCDP calculation more degrees of freedom are available to smooth out the dipole profile. Comparing the self-consistent dipole profile with the initially induced dipole profile of Fig. 1, one may notice not only a change in the numerical values but also a qualitative change in the shape. The initial charge density decreases monotonically away from the interface on both sides whereas the self-consistent profiles are oscillatory in character.

The monotonic character of the initial dipole profile can be understood from the fact that the charge transfer results from states near the top of the valence band. Because of the band discontinuity, states within the band continuum in one semiconductor lie within the gap of the other. The latter behaves as a barrier. When the two halves of the bicrystal are allowed to interact, some states in the gap become possible eigenstates of the heterojunction system. In other words, barrier penetration or charge transfer becomes possible. From this simple barrier-tunneling picture one clearly expects a monotonic and, in particular, an exponentially decaying charge transfer.

The self-consistent charge density is slightly oscillatory in character, overshooting on the first layer and compensating on the next layer. The third layer away from the interface is already neutral for all practical purposes,

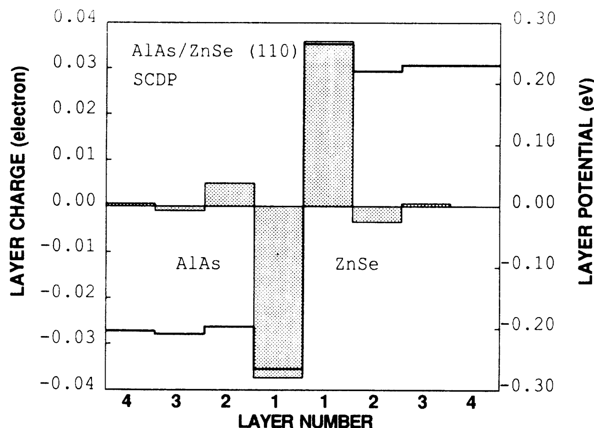

FIG. 6. Self-consistent layer charge (shaded) and associated electrostatic potential at the center of each layer (bold line) for ZnSe/AlAs (110). The latter is used as the constant shift of the otherwise frozen input potential, and is determined self-consistently.

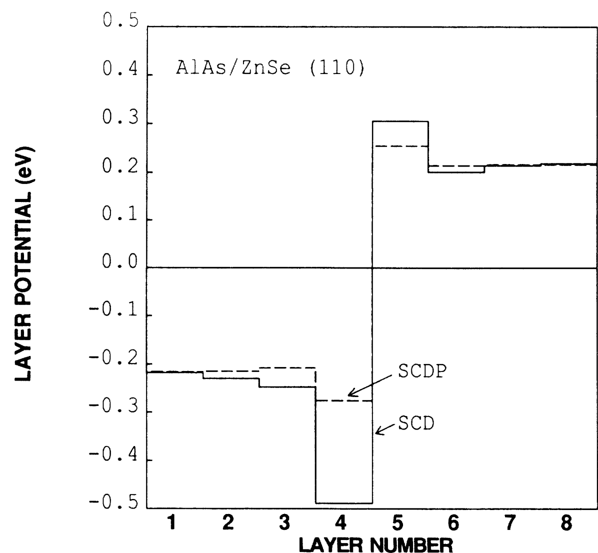

FIG. 7. Output-dipole profile obtained from a single-step input profile with the self-consistent value of the dipole (solid line), i.e., result of the SCD calculation, compared to the self-consistent dipole profile (dashed line), i.e., result of the SCDP calculation. In the first calculation only the dipole itself is made self-consistent, in the second the potential on each layer is made self-consistent.

showing that the induced charge density giving rise to the dipole is very localized near the interface and demonstrating the rapid cell-size convergence of the calculation. Larger oscillations are obtained in the SCD output than in the SCDP calculation. Similar oscillations have been obtained in tight-binding calculations by Harrison and Klepeis,[77] but seem to be absent or at least suppressed in the charge-density profiles obtained in pseudopotential calculations.[14–17] The latter are even more localized near the interface than in the present calculations. All of this is consistent with the notion that the more degrees of freedom that are taken into account for the charge density, the smoother and the more localized near the interface it becomes. The important message of this paper, however, is that this aspect of the calculation is irrelevant for the band offset, because all these differing calculations have the same dipole moment and thus asymptotic values of the potential. This also suggests the possibility that the oscillations (of small amplitude) in the dipole profile model obtained here may be an artifact of the limited number of degrees of freedom employed. It is also clear that whereas the dipole is screened by the macroscopic dielectric constant, a linear-response calculation of the full dipole profile would require a space-dependent dielectric function.

B. Results for band offsets

The results for the dipole correction and band offsets for a large number of (110) interfaces are summarized in Table I. The first column of this table gives the zeroth-order ASA reference-level lineup for the scalar-relativistic maximum of the valence bands calculated as discussed in Sec. III. The second column gives the spin-orbit correction and the third column gives the dipole correction calculated by means of the SCD approach. The values obtained by means of the SCDP approach are only included in parentheses for those cases in which a different result is obtained. The sum of these three contributions yields the valence-band offset within the SCD approach given in the fourth column. The values are compared with results of fully self-consistent LMTO calculations in column 5 and with other calculations and experiment in columns 6 and 7, respectively. The interface orientation for the experiment is indicated where different from (110). As already discussed in the Introduction, it makes sense to compare to the experimental data even if the latter do not correspond to the same interface orientation as the calculation, because the interface-orientation dependence is usually small.

From this table, it is evident that the dipole correction to the ASA lineup is generally a small but non-negligible correction (up to 0.7 eV). The overall uncertainty estimate of our calculation is of the order of 0.05–0.1 eV. This is mostly due to the LDA error in both the ASA values for the valence-band maximum and the LDA error in the dielectric constant and thus the dipole. Because the induced dipole is sensitive to the states at the top of the valence band, a compensating effect in the induced errors is expected. As pointed out earlier, the agreement between SCD and SCDP is very good, the largest discrepancy being 0.02 eV.

The agreement of the SCD and SCDP band offsets with the fully self-consistent LMTO calculations is also quite good, i.e., generally better than 0.1 eV. In a few cases the discrepancy is slightly larger (CuBr/AlAs, CuBr/ZnSe, ZnTe/GaSb). The largest discrepancy is 0.26 eV and occurs for CdTe/HgTe. As already pointed out in Sec. III there are several differences in the details of the calculation, and the extremely good agreement for the other cases is perhaps more remarkable than the few minor exceptions. It is also noteworthy that the final band offsets are in much better agreement than the initial ASA lineups, given in Ref. 8 and in the first column of our Table I. This indicates again that there is an important compensation between the magnitude of the dipole and the initial valence-band offset.

For CdTe/HgTe Christensen[18] reports insufficient convergence with cell size as a result of extended interface states. We checked our (7+7)-cell calculation with one for a (9+9)-cell and found agreement to within 0.001 eV for the dipoles. In fact, we obtain interface localized states similar to those found by Christensen. However, we have not pursued the study of their localization in as much detail as he did since our general theory implies that a single state, such as an interface localized state, would not have a significant effect on the dipole. The experimental situation is as follows. The value based on photoemission (0.35 eV) (Ref. 36) is close to our value, whereas the value based on modeling of the optical properties of quantum wells (0.04–0.12 eV) (Ref. 37) is much lower.

A recent calculation of Hui *et al.*[78] gives additional support for a high valence-band offset in CdTe/HgTe. They show that the magneto-optical experiment of Berroir *et al.*[79] which previously was interpreted in terms of a small valence-band offset (0.04 eV) can also, and, in fact, to better accuracy, be interpreted with a high valence-band offset of 0.35 eV.

Next, we compare our results to the pseudopotential calculations. Good agreement is found in some cases, but there are also significant discrepancies. These can be explained in terms of the different treatment of the shallow core d states.[18–20] The largest discrepancies occur for cases involving II-VI compounds (typically $\sim$0.6 eV), but those for Ga and In compounds are also not negligible ($\sim$0.1–0.3 eV). Although pseudopotential calculations do not neglect the shallow core d states entirely, their effect is only included indirectly through the construction of the nonlocal pseudopotential. In the case of II-VI compounds, the highest core d states lie $\sim$8 eV below the valence-band maximum, i.e., within the valence band. It is therefore important to include these orbitals explicitly into the Hamiltonian. The hybridization with these d states tends to push up the valence-band maximum and thus explains the signs of the deviations between the LMTO and pseudopotential calculations. Since the Ga or In d states lie $\sim$16 eV below the valence-band maximum, we found that these states can be treated adequately as frozen-core states. One might question why our LMTO calculations with a frozen core would give

TABLE I. Valence-band offsets and their contributions for (110) semiconductor heterojunctions: (i) Reference lineup (ASA); (ii) spin-orbit correction (S.O.); (iii) dipole calculated from a (7+7) superlattice by means of the SCD procedure (SCDP results in parentheses where different) (D); (iv) self-consistent-dipole result obtained as a sum of the first three columns (SCD); (v) fully self-consistent LMTO result from Ref. 18 for a (7+7) superlattice (LMTO); (vi) pseudopotential results for a (3+3) superlattice from Ref. 15 (PP); (vii) experimental results for (110) interfaces, except as indicated (Expt.). All energies in eV. The heterojunctions are grouped according to lattice constant. The common lattice constant used for each group is, respectively, 5.45, 5.65, 6.13, 6.48, 5.80, and 4.36 Å.

System	ASA[a]	S.O.	D	SCD	LMTO	PP	Expt.
GaP/Si	0.44	−0.01	−0.12	0.31	0.27	0.61	0.80[b]
AlP/Si	0.79	0.00	0.14(0.15)	0.93	0.91	1.03	
AlP/GaP	0.35	0.01	0.20	0.56	0.59	0.36	
GaAs/Ge	0.50	−0.02	−0.03	0.45	0.46	0.63	0.56[c]
AlAs/Ge	0.84	0.01	0.23(0.24)	1.08	1.03	1.05	0.95[d]
AlAs/GaAs	0.31	0.02	0.20	0.53	0.53	0.37[e]	0.42,[f,g] 0.55[h,g]
ZnSe/Ge	1.95	−0.05	−0.37(−0.38)	1.53	1.58	2.17	1.29–1.52[i]
ZnSe/GaAs	1.46	−0.04	−0.30	1.12	1.07	1.59	0.96−1.10[i]
ZnSe/AlAs	1.15	−0.06	−0.43	0.66	0.60		
CuBr/Ge[j]	1.80	0.04	−0.68(−0.70)	1.16	1.10		0.9[k]
CuBr/GaAs	1.27	0.06	−0.59(−0.60)	0.74	0.82		
CuBr/AlAs	0.96	0.04	−0.64(−0.66)	0.36	0.50		
CuBr/ZnSe	−0.19	0.10	−0.35	−0.44	−0.32		

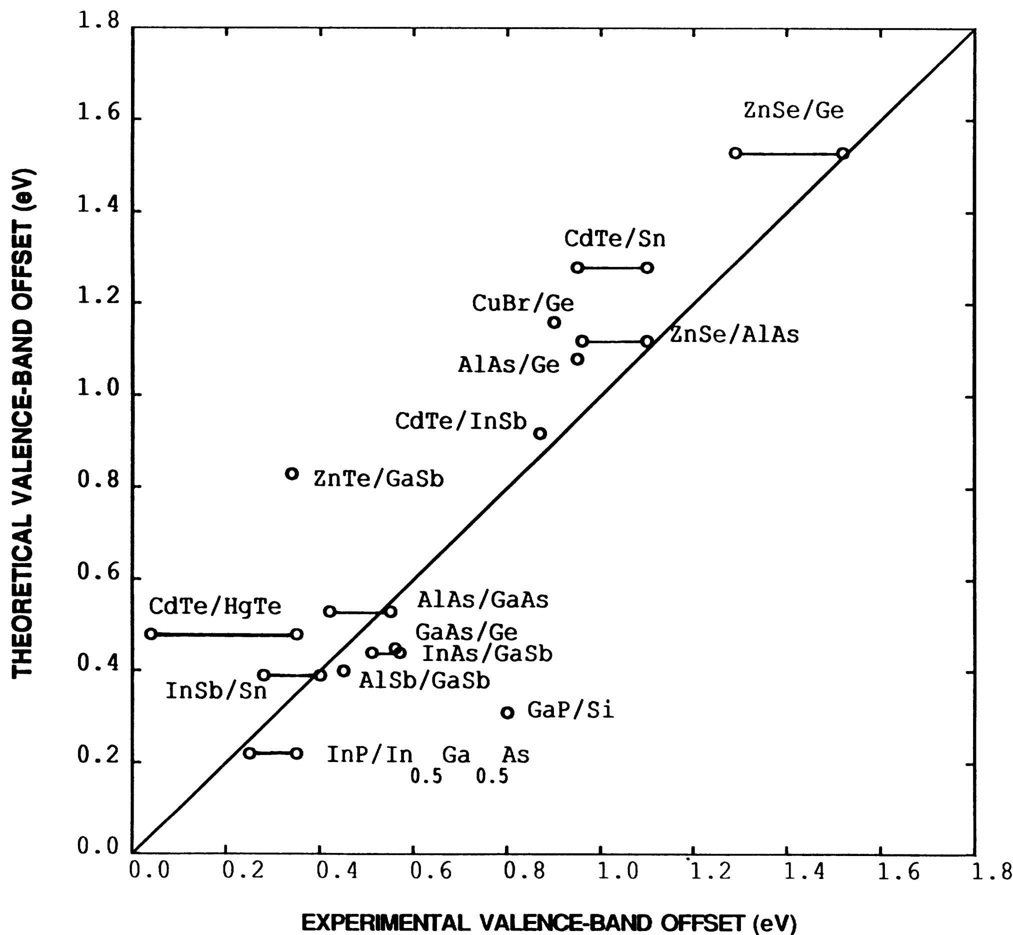

FIG. 8. Correlation between experimental and theoretical results for valence-band offsets (in eV). The spread on some of the experimental values is due either to different author's results as indicated in Table I or different conditions or samples from the same author's work. For details, the reader is referred to the original papers.

TABLE I. (*Continued*).

System	ASA[a]	S.O.	D	SCD	LMTO	PP	Expt.
InAs/GaSb	0.54	0.13	−0.23	0.44	0.46	0.38	0.51,[l,g] 0.57[m,g]
InAs/AlSb	0.36	0.10	−0.39	0.07			
AlSb/GaSb	0.18	0.03	0.19	0.40	0.45	0.38	0.45[n,g]
ZnTe/InAs	0.62	−0.20	0.13	0.55			
ZnTe/GaSb	1.17	−0.07	−0.14(−0.15)	0.96	0.83		0.34[o]
ZnTe/AlSb	0.98	−0.10	−0.28	0.60			
CdTe/Sn	1.66	−0.02	−0.36(−0.37)	1.28			0.95–1.1[p]
HgTe/Sn	1.28	−0.02	−0.60(−0.62)	0.66			
InSb/Sn	0.48	0.01	−0.10(−0.11)	0.39			0.28,[q] 0.40[r,g]
CdTe/HgTe	0.38	0.00	0.10	0.48	0.22	0.28	0.35,[s,t] 0.04–0.12[u,t]
CdTe/InSb	1.18	−0.03	−0.23(−0.24)	0.92	0.93		0.79[v]
HgTe/InSb	0.79	−0.03	−0.40(−0.41)	0.36	0.45		
$InP/In_{0.5}Ga_{0.5}As$[w]	0.04	0.06	0.12	0.22			0.25,[x,g] 0.35[y,g]
AlN/SiC[z]	1.86	0.00	−0.39(−0.40)	1.47			

[a] Including the combined correction.
[b] Reference 22.
[c] Reference 23.
[d] Reference 24.
[e] Similar pseudopotential calculations also for (110) 3+3 by other authors gave the results: 0.45 eV (Ref. 16) and 0.51 eV (Ref. 17). LAPW calculations for (001) 3+3 from Ref. 20 gave 0.5±0.05 eV and for 1+1 from Ref. 19 gave 0.42 eV.
[f] Reference 25.
[g] Experimental result for (001) interface.
[h] Reference 26.
[i] Reference 27.
[j] A two-panel calculation is used for the CuBr reference lineup but not for the dipole calculation.
[k] Reference 28.
[l] Reference 29.
[m] Reference 30.
[n] Reference 31.
[o] Reference 32.
[p] Reference 33.
[q] Reference 34.
[r] Reference 35.
[s] Reference 36.
[t] Experimental result for (111) interface.
[u] Reference 37.
[v] Reference 38.
[w] Virtual crystal average of InP/GaAs and InP/InAs both at lattice constant of InP ($a=5.80$ Å).
[x] References 39 and 79.
[y] Reference 40.
[z] Both in the sphalerite structure (note that AlN normally occurs in the closely related but hexagonal wurtzite structure and SiC exhibits various polytypes).

anything different from the pseudopotential calculation as they also incorporate the interaction with the lower-lying *d*'s only through their effect on the effective potential. In contrast to the pseudopotential calculations, however, the higher *d* partial waves incorporated in the description of the valence-band maximum are exactly orthogonal to the core states. Although the pseudopotentials are designed to achieve this orthogonality, the degree to which that is accomplished depends on the choice of the pseudopotential cutoff radius and the convergence of the plane-wave basis set. Exact orthogonalization is not guaranteed. Incomplete orthogonality to the lower *d* states would lower the top of the valence band and thus explain the difference between our frozen-core LMTO calculations and the pseudopotential calculations.

Our treatment of the Ga and In *d* states differs from Christensen's[18] which involved a two-panel calculation, and thus allowed for relaxation of the core *d* states. The present calculations seem to indicate that relaxing the core states is not essential for Ga or In. In fact, a simple perturbation theoretical argument shows that shifting these core states can only produce a very small effect on the valence-band maximum. Although in the actual calculation the effect of the core *d* states, both in our work

and in the two-panel calculation, is taken into account via the effective potential, we here discuss the effect in terms of a direct hybridization model to the core states. If the hybridization matrix element between the core state and the top of the valence band with energies ε_d and ε_v, respectively, is called H_{vd}, the shift of the valence-band top is in second-order perturbation theory given by

$$\Delta\varepsilon_v = \frac{|H_{vd}|^2}{\varepsilon_v - \varepsilon_d} . \quad (32)$$

A shift of the core level (due to relaxation) by $\delta\varepsilon_d$ will lead to a change in the shift of the valence-band maximum given by

$$\frac{\delta(\Delta\varepsilon_v)}{\Delta\varepsilon_v} \approx \frac{\delta\varepsilon_d}{\varepsilon_v - \varepsilon_d} . \quad (33)$$

Estimating $\delta\varepsilon_d \approx 0.5-1.0$ eV for Ga 3*d* or In 4*d*, the change in the hybridization shift of the top of the valence band due to relaxing the core states is seen to be at most $\sim 0.06\,\Delta\varepsilon_v$ where $\Delta\varepsilon_v$ itself is ~ 0.2 eV. This shows that the core relaxation is not very important for the present problem. Nevertheless, it has been found previously to affect total-energy properties such as the equilibrium lattice constant or the bulk modulus significantly. Note that the simple hybridization model used here is consistent with the fact that the discrepancy between LMTO and pseudopotential results is about twice as large for the II-VI compounds as for the III-V compounds because the *d* level lies twice as deep for the III-V compounds.

For the case of AlAs/GaAs a comparison can be made with several pseudopotential calculations[15–17] and also with linear-augmented-plane-wave[19,20] (LAPW) calculations. The latter included both the effect of the shallow core *d* states and the nonspherical contributions to the potential. With the exception of Van de Walle and Martin's calculation,[15] which gives 0.37 eV, all the methods essentially agree on a band offset of 0.5 ± 0.05 eV. Part of the uncertainty in this value is simply due to the different methods for extracting the band offset from the supercell potential involving different characteristics of the potential to relate the supercell calculation to the bulk calculations of the band structure. In the case of the LAPW calculations the core levels were used, while in the case of the pseudopotential calculations a suitable average of the pseudopotential, or of the electrostatic potential, is used. As noted above, we use the average point-charge potential defined within the ASA. Christensen uses the ASA potential wells of the bulklike layers of the supercell in a separate "frozen" calculation of the bulk band structure. Any reference level can, in principle, be used, but not all necessarily converge equally rapidly with increasing cell size. In the present calculation, the adequacy of this convergence was explicitly demonstrated.

Finally, we compare our results to the experimental values. An overview is provided in Fig. 8. The overall agreement is quite good, i.e., to within 0.15 eV. Two exceptions should be noted: GaP/Si and ZnTe/GaSb. In both cases, the various calculations are in better mutual agreement than any one of them with the experimental value. For GaP/Si, the pseudopotential calculation is in better agreement with experiment than are the LMTO or SCDP calculations. However, this must be considered questionable as the pseudopotential result suffers from the *d*-band problem discussed above. This suggests that experimental artifacts or complications in the samples, such as nonideal interfaces, atomic intermixing, etc., may be responsible for these discrepancies with the calculations. Further measurements for these interfaces are desirable.

V. CONCLUDING REMARKS

The main thesis proposed in this paper is that band offsets can be obtained from a single-parameter variational calculation of the total energy within the framework of density-functional theory in the local-density approximation. We emphasize that no meaningful absolute reference level exists for the lineup of the potentials of different solids. Nevertheless, starting from any chosen lineup the correct self-consistent lineup is obtained within linear response by dielectrically screening the initially induced interface dipole. The screening involves the macroscopic dielectric constant of the heterojunction interface region. The initially induced dipole is obtained by performing a single iteration cycle: i.e., calculating the band structure for the heterojunction and subsequently the dipole from the resulting charge density once, starting from the bulk potentials with the given lineup. It was shown that a fully self-consistent calculation is essentially equivalent to dividing this dipole by the macroscopic dielectric constant of the heterojunction interface region. The latter was shown to be approximately given by the harmonic average of the dielectric constants of the two semiconductors. In addition, it was shown that the single-parameter calculation readily provides this macroscopic dielectric constant via the slope of the input-output curve of the dipoles to within the accuracy of the LDA, i.e., $\sim 10\%$. This is related to the nature of the dielectric response which is much larger for long-range than for short-range components of the perturbation and to the smallness of the off-diagonal (between long-range and short-range) components of the dielectric matrix in real space. The extensive set of calculations provides convincing numerical proof of the above statements for practical purposes. Detailed comparisons of the results at different levels of approximation were used to illustrate the various aspects of this work. The practical usefulness of the theory for the band-offset problem is demonstrated by the satisfactory agreement with available experimental data and other more involved calculations in the literature.

The present theory provides valuable new insights into the origin of band offsets. For example, it explains how the band offset can at the same time be an interface-dependent quantity in a fundamental and principle sense and still be fairly independent to interface orientation. The reason is simply that any interface-related change in the initially induced dipole (which in many cases is already small because of similar bonding configurations) will be screened by the large macroscopic dielectric constant of the semiconductors. The insensitivity of the

band offsets to interface structure or orientation should, therefore, not be taken as a justification for postulating the existence of a meaningful absolute reference level. The interface orientation dependence will be discussed in a future paper[46] but preliminary results indicate it to be small for all isovalent systems and, in particular, common-anion systems.[45] Important interface composition and structure dependence, however, have been shown to exist for nonisovalent systems.[4,5,14,45–47]

Although the present numerical calculations focused on semiconductor heterojunctions, one might attempt to apply the same theory to metal-semiconductor and metal-metal contacts. The validity of linear response seems to be more questionable in these cases and practical difficulties arise in estimating the large dielectric screening in a system with a metallic nature. If one attempts to use the SCD model, it may be necessary to use an iterative procedure whereby one gradually would approach the linear-response region through successive approximations. Also, a word of caution is required here concerning the use of the LDA. Whereas for semiconductor heterojunctions, the errors due to the LDA tend to cancel out because they are comparable on both sides, the different natures of metals and semiconductors may lead to a reinforcement of the LDA errors[61] for interfaces between these materials. For metal-metal contacts the application of the present theory is rather trivial. Because both dielectric constants are infinite no long-range dipole can exist in the system. This simply means that local charge neutrality must be assured by aligning the Fermi level. Any attempt to calculate the infinite macroscopic dielectric constant in this case will result in strong nonlinear behavior.

Even for semiconductor heterojunctions, we have indicated that the macroscopic dielectric constants have LDA errors of $\sim 10\%$ or even larger for the more ionic semiconductors. This leads to uncertainties of the dipole of the order of 0.01–0.05 eV. However, one should note that the originally induced dipole is related to the initial band offset, which depends on the energy band position with respect to the average electrostatic point-charge potential and is thus also sensitive to LDA errors. As the initially induced dipole clearly is sensitive to the states at the top of the valence band, i.e., to the initial lineup, one expects a compensating effect: the higher the initial band offset, the higher the compensating dipole. This means that, in our opinion, one should *not* include quasiparticle self-energy corrections to the band edges without at the same time recalculating the dipole with exchange correlation treated beyond LDA. In fact, in exact density-functional theory the valence-band maximum quasiparticle should equal the corresponding Kohn-Sham eigenvalue. For lack of an exact exchange-correlation potential, it seems preferable, for the time being, to be at least consistent in the approximations for the valence-band maximum and the dipole, which are both ground-state properties.

The proof of the main thesis of the present paper is largely based on a careful analysis of the nature of self-consistent calculations in terms of linear-response theory and on the idea of restricted variational freedom calculations within the density-functional theory. These ideas are applicable in a much wider context and, e.g., are also extremely useful for evaluating total-energy properties, such as energy of formation of alloys, interfaces, and superlattices. These themes are planned to be explored in future work.

Note added in proof. We have reinvestigated the particularly sensitive case of the CdTe/HgTe valence-band offset with improved accuracy, using a larger number of **k** points and treating the dipole and the ASA reference-level band offset completely on equal footing. The result was 0.36 eV, in excellent agreement with the photoemission experiment.[36] Details will be published elsewhere.

ACKNOWLEDGMENTS

Stimulating discussions with P. Blöchl, N. E. Christensen (who provided us with many of his results prior to publication), R. M. Martin, and C. G. Van de Walle are gratefully acknowledged. One of us (W.R.L.L.) would like to express thanks for the hospitality at the Max-Planck-Institut für Festkörperforschung, where this work was started, and is especially indebted to O. Jepsen, who introduced him to the practical aspects of LMTO calculations and provided him with the basic LMTO-program package. He is also indebted to R. Resta and S. Baroni for useful discussions of local-field effects in dielectric screening. The work at Case Western Reserve University was supported by the U.S. Defense Advanced Research Projects Agency, Office of Naval Research, University Research Initiative Contract No. N000-13-86-K-0773. Partial support was also provided by NASA Lewis Research Center Grant No. NAG 3-954. Computing time was provided by the Pittsburgh Supercomputing Center, Grant No. PHY870036P.

[1] R. L. Anderson, Solid-State Electron. **5**, 341 (1962).

[2] W. R. Frensley and H. Kroemer, J. Vac. Sci. Technol. **13**, 810 (1976); Phys. Rev. B **16**, 2642 (1977).

[3] W. A. Harrison, *Electronic Structure and Properties of Solids* (Freeman, San Francisco, 1980).

[4] W. A. Harrison, E. A. Kraut, J. R. Waldrop, and R. W. Grant, Phys. Rev. B **18**, 4402 (1978).

[5] R. W. Grant and W. A. Harrison, J. Vac. Sci. Technol. B **6**, 1295 (1988).

[6] C. Tejedor and F. Flores, J. Phys. C **11**, L19 (1978); F. Flores and C. Tejedor, *ibid.* **12**, 731 (1979).

[7] J. Tersoff, Phys. Rev. Lett. **30**, 4874 (1984); J. Vac. Sci. Technol. B **4**, 1066 (1986).

[8] M. Cardona and N. E. Christensen, Phys. Rev. B **35**, 6182 (1987).

[9] M. Jaros, Phys. Rev. B **37**, 7112 (1988).

[10] W. A. Harrison and J. Tersoff, J. Vac. Sci. Technol. B **4**, 1068 (1986).

[11] I. Lefebvre, M. Lannoo, C. Priester, G. Allan, and C. Delerue, Phys. Rev. B **36**, 1336 (1987).

[12] B. Haussy, C. Priester, G. Allan, and M. Lannoo, Phys. Rev. B **36**, 1105 (1987); C. Priester, G. Allan, and M. Lannoo, *ibid.* **33**, 7386 (1986); J. Vac. Sci. Technol. B **6**, 1290 (1988).

[13] F. Flores and C. Tejedor, J. Phys. C **20**, 145 (1987), and references therein; A. Muñoz, J. Sánchez-Dehesa, and F. Flores, Phys. Rev. B **35**, 6468 (1987); J. C. Durán, F. Flores, C. Tejedor, and A. Muñoz, *ibid.* **36**, 5920 (1987); G. Platero, J. Sánchez-Dehesa, C. Tejedor, and F. Flores, Surf. Sci. **168**, 553 (1986); J. C. Durán, A. Muñoz, and F. Flores, Phys. Rev. B **35**, 7721 (1987).

[14] K. Kunc and R. M. Martin, Phys. Rev. B **24**, 3445 (1981).

[15] C. G. Van de Walle and R. M. Martin, Phys. Rev. B **35**, 8154 (1987); **37**, 4801 (1988); C. G. Van de Walle, Ph.D. thesis, Stanford University, 1986 (unpublished); Phys. Rev. B **39**, 1871 (1988).

[16] D. M. Bylander and L. Kleinman, Phys. Rev. Lett. **59**, 2091 (1987); Phys. Rev. B **36**, 3229 (1987).

[17] A. Baldereschi, S. Baroni, and R. Resta, Phys. Rev. Lett. **61**, 734 (1988).

[18] N. E. Christensen, Phys. Scr. **T19**, 298 (1987); Phys. Rev. B **37**, 4528 (1988); **38**, 12 687 (1988); N. E. Christensen and L. Brey, *ibid.* **38**, 8185 (1988).

[19] S.-H. Wei and A. Zunger, Phys. Rev. Lett. **59**, 144 (1987).

[20] S. Massidda, B. I. Min, and A. J. Freeman, Phys. Rev. B **35**, 9871 (1987).

[21] W. R. L. Lambrecht and B. Segall, Phys. Rev. Lett. **61**, 1764 (1988).

[22] P. Perfetti, F. Patella, F. Settle, C. Quaressima, F. Capasso, A. Savoia, and G. Margaritondo, Phys. Rev. B **30**, 4533 (1984).

[23] J. R. Waldrop, E. A. Kraut, S. P. Kowalczyk, and R. W. Grant, Surf. Sci. **132**, 513 (1983).

[24] G. Margaritondo, Phys. Rev. B **31**, 2526 (1985).

[25] J. Menéndez, A. Pinczuk, D. J. Werder, A. C. Gossard, and J. H. English, Phys. Rev. B **33**, 8863 (1986).

[26] J. Batey and S. L. Wright, J. Appl. Phys. **59**, 1200 (1986).

[27] S. P. Kowalczyk, E. A. Kraut, J. R. Waldrop, and R. W. Grant, J. Vac. Sci. Technol. **21**, 482 (1982).

[28] R. S. Bauer and G. Margaritondo, Phys. Today **40** (1), 27 (1987).

[29] J. Sakaki, L. L. Chang, R. Ludeke, C. A. Chang, G. A. Sai-Halasz, and L. Esaki, Appl. Phys. Lett. **57**, 2556 (1977).

[30] L. M. Claessen, J. C. Maan, M. Altarelli, P. Wyder, L. L. Chang, and L. Esaki, Phys. Rev. Lett. **57**, 2556 (1986).

[31] J. Menéndez, A. Pinczuk, D. J. Werder, J. P. Valladares, T. H. Chiu, and W. T. Tsang, Solid State Commun. **61**, 703 (1987).

[32] W. G. Wilke and K. Horn, J. Vac. Sci. Technol. B **6**, 1211 (1988).

[33] H. Höchst, D. W. Niles, and I. Hernandez-Calderon, J. Vac. Sci. Technol. B **6**, 1219 (1988).

[34] A. Förster, A. Tulke, and H. Lüth, J. Vac. Sci. Technol. B **5**, 1054 (1987).

[35] P. John, T. Miller, and T.-C. Chiang, Phys. Rev. B **39**, 3223 (1989).

[36] S. P. Kowalczyk, J. T. Cheung, E. A. Kraut, and R. W. Grant, Phys. Rev. Lett. **56**, 1605 (1986).

[37] D. J. Olego, J. P. Faurie, and P. M. Racah, Phys. Rev. Lett. **55**, 328 (1985).

[38] K. J. Mckey, P. M. G. Allen, W. G. Herrender-Harker, R. H. Williams, C. R. Whitehouse, and G. M. Williams, Appl. Phys. Lett. **49**, 354 (1986).

[39] R. Sauer, T. D. Harris, and W. T. Tsang, Phys. Rev. B **34**, 9023 (1986).

[40] D. V. Lang, M. B. Panish, F. Capasso, J. Allam, R. A. Hamm, A. M. Sergent, and W. T. Tsang, Appl. Phys. Lett. **50**, 736 (1987).

[41] S. B. Zhang, D. Tománek, S. G. Louie, M. L. Cohen, and M. S. Hybertsen, Solid State Commun. **66**, 585 (1988).

[42] M. S. Hybertsen and M. Schlüter, Phys. Rev. B **36**, 9683 (1987).

[43] L. Kleinman, Phys. Rev. B **24**, 7412 (1981).

[44] O. K. Andersen, Phys. Rev. B **12**, 3060 (1975); O. K. Andersen, O. Jepsen, and D. Glötzel, in *Highlights of Condensed Matter Theory,* edited by F. Bassani, F. Fumi, and M. P. Tosi (North-Holland, Amsterdam, 1985), p. 59; O. K. Andersen, O. Jepsen, and M. Šob, in *Electronic Band Structure and Its Applications,* edited by M. Yussouff (Springer, Heidelberg, 1987).

[45] W. R. L. Lambrecht and B. Segall, Bull. Am. Phys. Soc. **34**, 878 (1989).

[46] W. R. L. Lambrecht and B. Segall, following paper, Phys. Rev. B **41**, 2832 (1990).

[47] S. Satpathy and R. M. Martin, Phys. Rev. B **39**, 8494 (1989).

[48] P. Perfetti, Q. Quaresima, C. Coluzza, C. Fortunato, and G. Margaritondo, Phys. Rev. Lett. **57**, 2056 (1986); D. W. Niles, G. Margaritondo, P. Perfetti, C. Quaresima, and M. Capozi, Appl. Phys. Lett. **47**, 1092 (1985); D. W. Niles, E. Colativa, G. Margaritondo, P. Perfetti, C. Quaresima, and M. Capozi, J. Vac. Sci. Technol. A **4**, 962 (1986).

[49] The semiempirically fitted tight-binding Hamiltonians are usually only defined with energies relative to the top of the valence band, so that additional assumptions must be made to obtain the diagonal energies with respect to a common reference level. Atomic energy levels have, e.g., been used. The authors of Ref. 12 avoid a definite choice by replacing the self-consistency requirement with a more approximate local-charge-neutrality requirement.

[50] P. Hohenberg and W. Kohn, Phys. Rev. **136**, B864 (1964).

[51] W. Kohn and L. J. Sham, Phys. Rev. **140**, A1133 (1965).

[52] L. J. Sham and W. Kohn, Phys. Rev. **145**, 561 (1966); C. -O. Almbladh and U. von Barth, Phys. Rev. B **31**, 3231 (1985).

[53] J. P. Perdew and M. Levy, Phys. Rev. Lett. **51**, 1884 (1983).

[54] L. J. Sham and M. Schlüter, Phys. Rev. Lett. **51**, 1888 (1983).

[55] M. S. Hybertsen and S. G. Louie, Phys. Rev. Lett. **55**, 1418 (1985); Phys. Rev. B **34**, 5390 (1986).

[56] R. W. Godby, M. Schlüter, and L. J. Sham, Phys. Rev. Lett. **56**, 2415 (1986); Phys. Rev. B **37**, 10 159 (1988).

[57] O. Gunnarsson and K. Schönhammer, Phys. Rev. Lett. **56**, 1968 (1986).

[58] J. A. Vergés, D. Glötzel, M. Cardona, and O. K. Andersen, Phys. Status Solidi B **113**, 519 (1982).

[59] O. K. Andersen (unpublished).

[60] This concept was developed through discussions with P. Blöchl.

[61] G. P. Das, P. Blöchl, O. K. Andersen, N. E. Christensen, and O. Gunnarsson, Phys. Rev. Lett. **63**, 1168 (1989).

[62] J. Kollar and O. K. Andersen (unpublished), referred to in Andersen, Jepsen, and Glötzel (Ref. 44).

[63] H. L. Skriver, Phys. Rev. B **31**, 1909 (1985).

[64] A. K. McMahan and J. A. Moriarty, Phys. Rev. B **27**, 3235 (1983).

[65] O. K. Andersen and N. E. Christensen (unpublished), referred to in N. E. Christensen and O. B. Christensen, Phys. Rev. B **33**, 4739 (1986).

[66]A. R. Mackintosh and O. K. Andersen, in *Electrons at the Fermi Surface,* edited by M. Springford (Cambridge University Press, Cambridge, 1980); also see V. Heine, in *Solid State Physics,* edited by F. Seitz and D. Turnbull (Academic, New York, 1980), Vol. 35, p. 1.

[67]W. R. L. Lambrecht and B. Segall, in *Proceedings of the Acta/Scripta Metallurgica Conference on Bonding, Structure and Mechanical Properties of Metal/Ceramic Interfaces,* edited by M. F. Ashby, A. G. Evans, J. P. Hirth, and M. Rühle (Pergamon, Oxford, 1989).

[68]R. Resta and K. Kunc, Phys. Rev. B **34**, 7146 (1986).

[69]W. R. L. Lambrecht and B. Segall, Phys. Rev. B **40**, 7793 (1989).

[70]M. S. Hybertsen and S. H. Louie, Phys. Rev. B **35**, 5585 (1988).

[71]P. K. W. Vinsome and D. Richardson, J. Phys. C **4**, 2650 (1971).

[72]W. R. L. Lambrecht and O. K. Andersen, Surf. Sci. **178**, 256 (1986), and unpublished.

[73]H. J. Monkhorst and H. D. Pack, Phys. Rev. B **13**, 5188 (1976).

[74]D. J. Chadi and M. L. Cohen, Phys. Rev. B **8**, 5747 (1973).

[75]*Landolt-Börnstein: Numerical Data and Functional Relationships in Science and Technology, New Series,* edited by O. Madelung (Springer, Berlin, 1982), Vol. 17a.

[76]C. G. Broyden, Math. Comput. **19**, 577 (1965).

[77]W. A. Harrison and J. E. Klepeis, Phys. Rev. B **37**, 864 (1988).

[78]P. M. Hui, H. Ehrenreich, and N. F. Johnson, J. Vac. Sci. Technol. A **7**, 424 (1989).

[79]J. M. Berroir, Y. Guldner, J. P. Vieren, M. Voos, and J. P. Faurie, Phys. Rev. B **34**, 891 (1986); Y. Guldner, G. Bastard, J. P. Vieren, M. Voos, J. P. Faurie, and A. Million, Phys. Rev. Lett. **51**, 907 (1983).

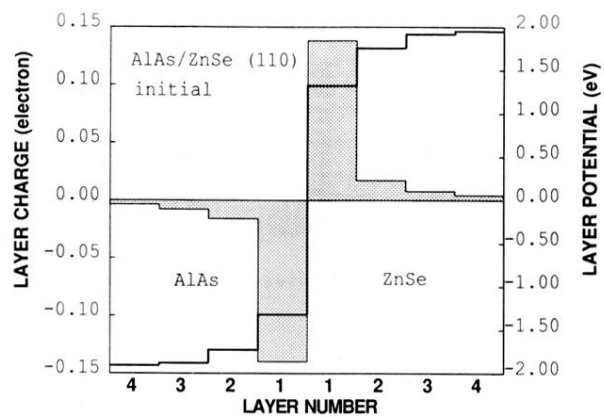

FIG. 1. Initially induced layer charge (shaded) and associated electrostatic potential at the center of each layer (bold line) for ZnSe/AlAs (110) starting from the ASA lineup. Each layer contains a cation, an anion, and two empty spheres, and is neutral in the bulk.

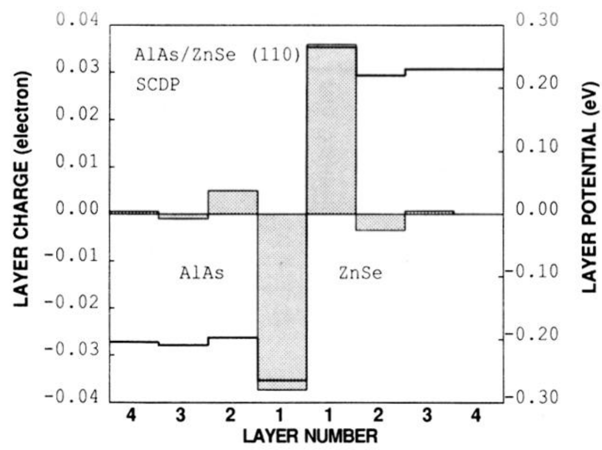

FIG. 6. Self-consistent layer charge (shaded) and associated electrostatic potential at the center of each layer (bold line) for ZnSe/AlAs (110). The latter is used as the constant shift of the otherwise frozen input potential, and is determined self-consistently.